ACS OMEGA

http://pubs.acs.org/journal/acsodf

Article

Highly Efficient Industrial Dye Degradation, Bactericidal Properties, and *In Silico* Molecular Docking Analysis of Ag/Cellulose-Doped CuO Nanostructures

Muhammad Ikram,* Izan Hafeez, Misbah Naz, Ali Haider, Sadia Naz, Anwar Ul-Hamid,* Junaid Haider, Anum Shahzadi, Muhammad Imran, Walid Nabgan,* and Salamat Ali

Cite This: *ACS Omega* 2022, 7, 17043−17054

Read Online

ACCESS | Metrics & More | Article Recommendations | Supporting Information

ABSTRACT: In this research, CuO nanostructures doped with Ag and cellulose nanocrystals (CNC) were synthesized using a facile coprecipitation technique. In this work, we doped Ag into fixed quantities of CNC and CuO to improve the photocatalytic, catalytic, and antibacterial activity. It was noted that catalytic activity increased upon doping, which was attributed to the formation of nanorods and a pH effect, while the reverse trend was observed in photocatalytic activity. The addition of Ag and CNC dopants into CuO improved the bactericidal efficacy for *S. aureus* and *E. coli*. In addition, to obtain insight into the possible mechanism behind their biocidal effects, molecular docking studies were conducted against specific enzyme targets: namely, dihydrofolate reductase from *E. coli* and DNA gyrase from *S. aureus*. This study suggested that codoped CuO could be highly efficient in the cleaning of polluted water and antibacterial applications.

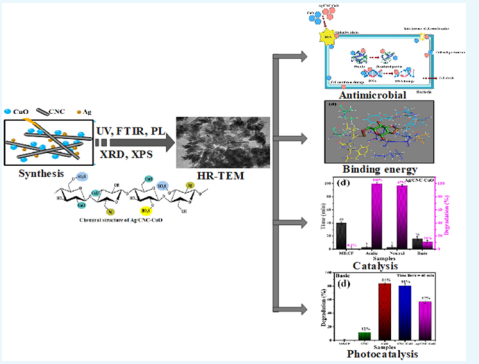

1. INTRODUCTION

Water is an essential nutrient for life, but merely 2.5% of water is appropriate for human consumption, and the remaining 97.5% is salty water. With rampant population growth, potable water resources are being continuously depleted, posing severe challenges to the survival of living species.[1,2] By 2050, the earth's population is expected to reach 9.0 billion, and by 2075, 75% of humankind may face water scarcity, according to the United Nations Water Agency report.[3] Aquatic pollution triggered by human waste causes adverse conditions.[4−6] Every year, industries produce around 7 x 10^5 tons dyes. Among them, 10−15% of methylene blue (MB) is discharged in water bodies annually, which can cause harmful diseases, including cancer, kidney malfunction, skin irritation, and hepatitis.[7,8] Moreover, ciprofloxacin (CF), detected in wastewater discharged from hospitals and medical industries and employed to treat infectious diseases, is a threat to the aquatic environment with concentrations of up to 150 μg/L and 31−50 mg/L, respectively.[9,10] In a nutshell, living resources are seriously endangered due to the phototoxicity, bioavailability, and aquatic toxicity of synthetic dyes and medicines.[11]

Due to these hazardous effects, toxic pollutants in water need to be controlled to preserve freshwater resources.[12] Intense studies have been undertaken to develop techniques to prevent domestic and industrial pollutants from affecting the environment.[13,14] The advanced oxidation processes include supercritical water oxidation, electrochemical oxidation, Fenton reactions, wet air oxidation, catalysis, and photocatalysis.[15] Among these techniques, catalysis and photocatalysis are effective and environmentally friendly techniques that have been utilized to degrade dyes for many years.[7,16]

Metal oxide nanoparticles (MONPs) are potential candidates for pollutant removal. In recent years, many MONPs (ZnO, CaO, TiO_2, SnO_2, and CuO) have been utilized as active catalysts.[17] Among the multiple MONPs, copper oxide (CuO) nanoparticles (NPs) are used because of their natural abundance, nontoxic nature, low-cost production, high thermal stability, and better electrical and optical characteristics.[18] As a narrow-band-gap p-type semiconductor, CuO has various applications that include solar energy conversion, the water-gas shift reaction, field emission, superconducting materials, sensing materials, glass, and ceramics.[19] Narrow-band-gap semiconductors exhibit superior antimicrobial properties and are powerful heterogeneous catalysts when they are integrated with coatings.[14] For this purpose, unique structures can provide a larger surface area and increase active sites for photocatalytic dye degradation. In this respect, many researchers have utilized a biopolymer (cellulose) for the enhancement of MONP properties.[20]

Received: January 12, 2022
Accepted: April 26, 2022
Published: May 9, 2022

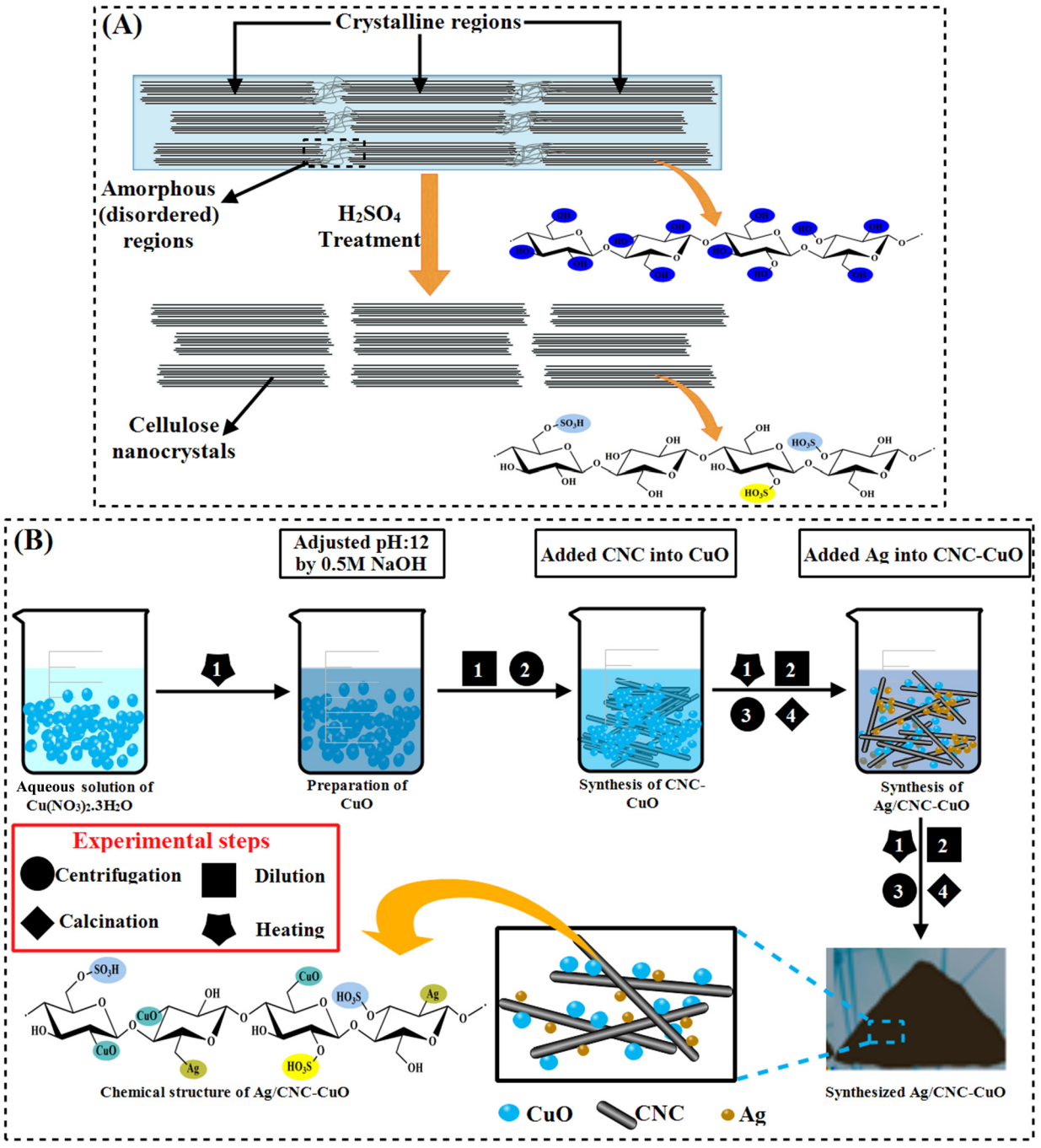

Figure 1. (A) CNC synthesis from cellulose microfibrils, having crystalline and amorphous regions, by sulfuric acid hydrolysis. The synthesized CNC surface contained sulfate ester groups formed as a side reaction. (B) Schematic of the preparation and structure of Ag/CNC-CuO nanostructures.

Currently, biopolymers, in terms of their efficient, sustainable, and environmentally friendly nature, are favorable building blocks for developing high-performance hybrid materials.[21,22] Cellulose is an innovative material and an abundantly available polysaccharide on earth, and its low-cost availability, biocompatibility, chemical stability, and ease of biodegradation offer a potential material for a variety of applications.[23−26] Cellulose nanocrystals (CNCs) also offer versatile surface chemistry that promotes the growth of various NPs, such as metal−organic frameworks (MOFs) and MONPs.[21,27] Cellulose-nanostructure-based characteristics lead to the strong binding of inorganic semiconductors on the surface, supporting the high stability of nanomaterials.[28−30]

The introduction of inorganic metal nanoparticles such as Ag, Au, Cu, and Zn NPs into cellulose has been a widely used approach to enhance antibacterial activity throughout the years.[23] Specifically, Ag has been given significant attention because of its potent antimicrobial and dye degradation activity due to its high surface to volume ratio.[23,24,31] Furthermore, a photocatalytic control sample (CuO) is boosted by coupling with transition metals, limiting photoinduced electron−hole recombination and increasing the band-gap energies.[14,32,33] It

https://doi.org/10.1021/acsomega.2c00240
ACS Omega 2022, 7, 17043−17054

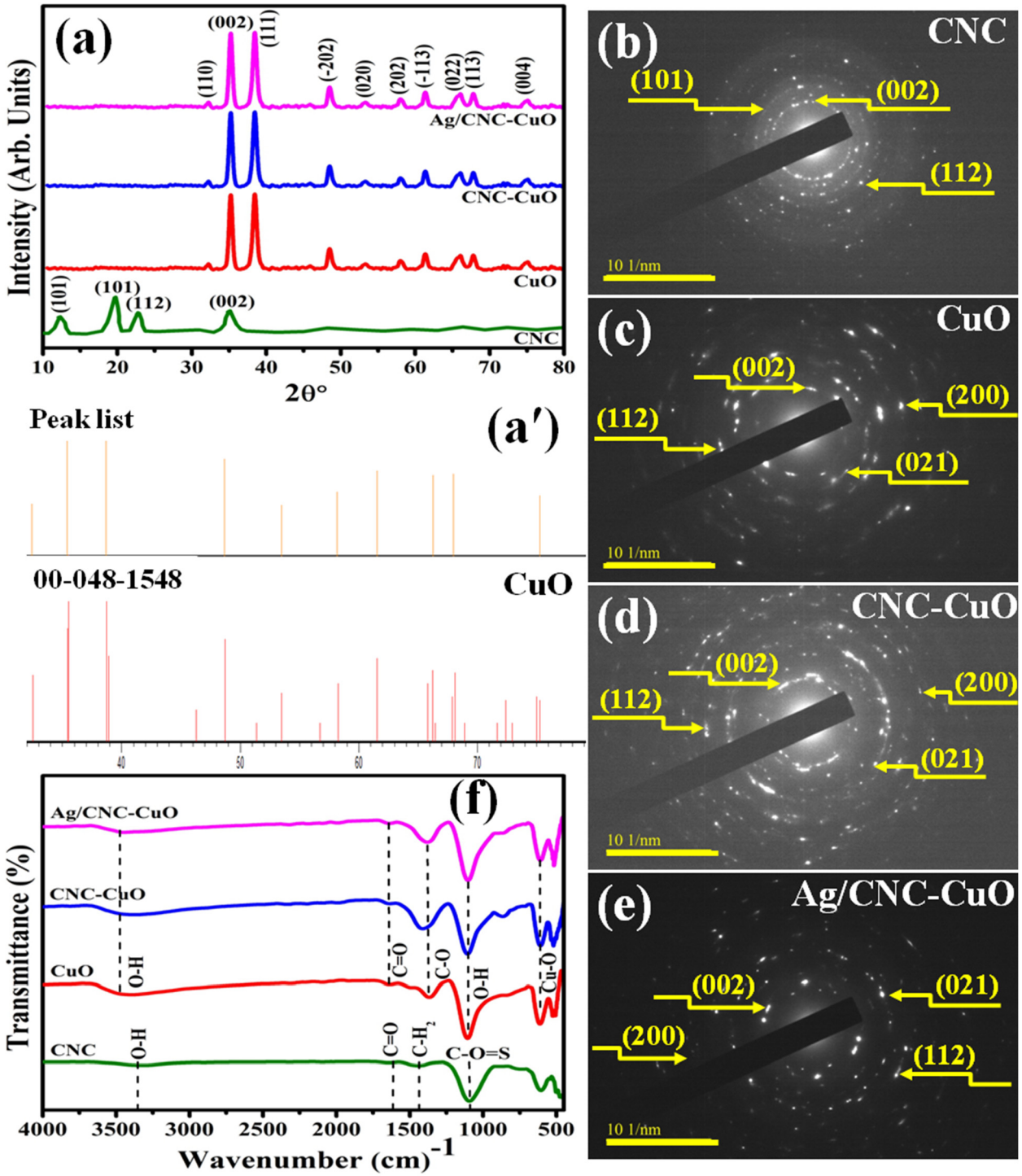

Figure 2. (a) XRD analysis of Ag/CNC-CuO. (a′) Reference code of CuO. (b−e) SAED patternd of CNC, CuO, CuO−CNC, and Ag/CNC-CuO, respectively. (f) FTIR spectra of the samples.

is reported that silver doping remarkedly improves the photocatalytic activity of semiconductor NPs.[14,34]

This study focuses on developing a facile approach for the eco-friendly degradation of industrial effluents and providing a strategy to control microbes. Ag- and cellulose-doped CuO nanostructures (Ag/CNC-CuO) were fabricated via a coprecipitation method for the photocatalytic and catalytic degradation of MB:CF and generating antimicrobial activity against Gram (positive and negative) bacteria. To understand how CNC-CuO NPs and Ag/CNC-CuO NPs kill bacteria, molecular docking experiments were performed on *E. coli* dihydrofolate reductase (DHFR) and *S. aureus* DNA gyrase enzymes.

2. MATERIALS AND METHODS

Details of the materials used coupled with their suppliers, experimental protocols used in this study for determining the catalytic potential, photocatalysis, antimicrobial activity against identified strains of *E. coli* and *S. aureus*, and molecular docking analyses of the prepared samples are presented in the

https://doi.org/10.1021/acsomega.2c00240
ACS Omega 2022, 7, 17043−17054

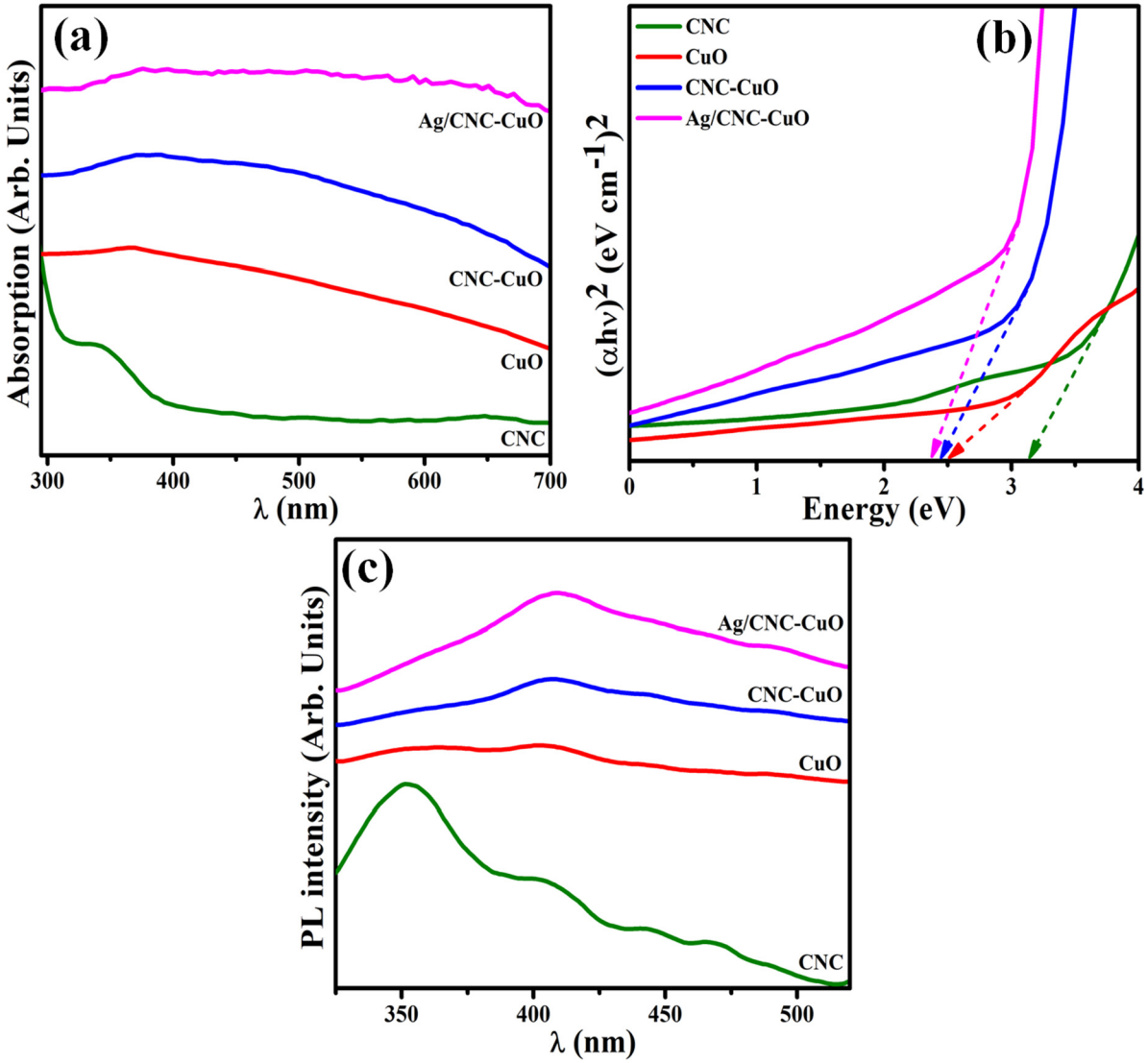

Figure 3. (a) Absorption spectra, (b) band-gap energy plot, and (c) PL spectra.

Supporting Information. Moreover, various techniques used for the extensive characterization of synthesized samples, including XRD, FTIR, ultraviolet−visible spectrophotometry, PL analysis, and HR-TEM, are also described in theSupporting Information.

2.1. Synthesis of Cellulose Nanocrystals (CNCs). First, Avicel (10 g) added to a 50% solution of concentrated H_2SO_4 and DI water (200 mL) was stirred at 45 °C for 30 min to synthesize CNCs (Figure 1a). Subsequently, 5 L of DI water was incorporated to dilute H_2SO_4, and the supernatant was collected. To control the pH of the collected solution from acidic to neutral, an NaOH (0.5 M) solution was used. This neutral solution was centrifuged three times at 7100 rpm for 9 min.[35] The centrifuged CNC solution with neutral pH was dried for 7 h at 100 °C for further study. The obtained CNC in powder form had a concentration of 117 mg/mL.

2.2. Synthesis of Ag/Cellulose-Doped CuO. The CuO nanomaterial was synthesized via a coprecipitation method (Figure 1b). Initially, the Cu source was 0.1 M of $Cu(NO_3)_2 \cdot 3H_2O$ was prepared with constant stirring. After that, an NaOH (0.5 M) solution was incorporated drop by drop into the colloidal solution to fix the pH to 12 with vigorous stirring at 90 °C for 30 min.[36] DI water (150 mL) was added, and the mixture was centrifuged three times to extract nitrate from the solution. A 2.5 wt % portion of CNC was added to the prepared CuO solution, and the mixture was heated at 95 °C for 30 min. Later, 150 mL of water was poured into the doped solution and the mixture was centrifuged three times and calcinated at 120 °C. Finally, 2% Ag was doped into the CNC-CuO solution by adding $AgNO_3$ as a precursor and the mixture was stirred at around 90 °C and centrifuged two times. The obtained precipitates were dried at 120 °C for 7 h and ground well with a mortar and pestle.

3. RESULTS AND DISCUSSION

The crystal structures, sizes, and phase compositions of CNC, CuO, CNC-CuO, and Ag/CNC-CuO were determined using X-ray diffraction (Figure 2a). The observed diffraction pattern for CNC revealed peaks positioned at 12, 19.5, 22.4, and 33.9° assigned to (101), (101), (002), and (112) crystal planes, respectively, and exhibited a monoclinic structure consistent with JCPDS card 46-0905.[37,38] Peaks found at 32.2, 35.3, 38.2, 48.3, 53.2, 58.1, 61.2, 66.04, 67.9, and 75.1° indexed as (110), (002), (111), (−202), (020), (202), (−113), (022), (113,)

https://doi.org/10.1021/acsomega.2c00240
ACS Omega 2022, 7, 17043−17054

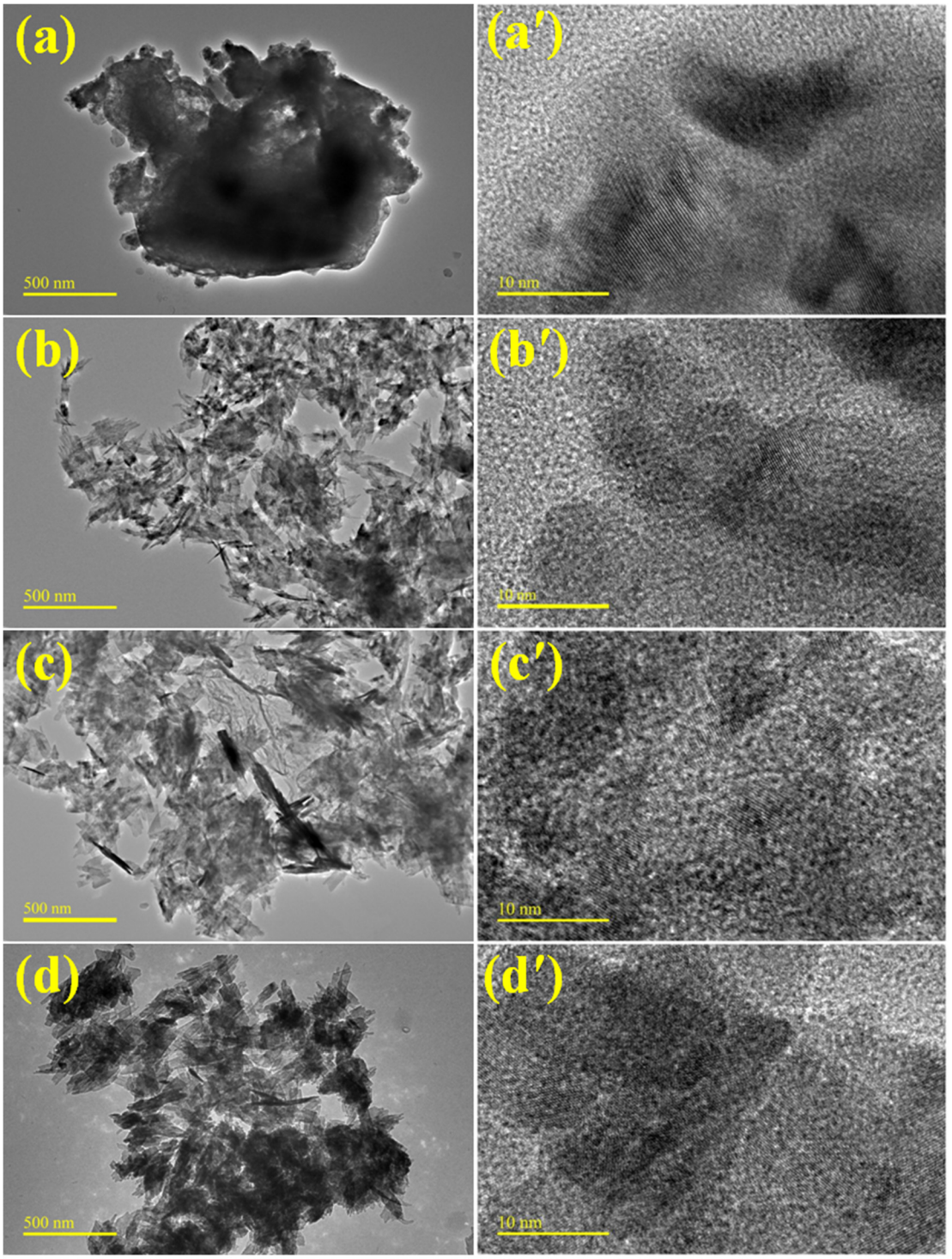

Figure 4. (a−d) HR-TEM images of CNC, CuO, CNC-CuO, and Ag/CNC-CuO, respectively on a 500 nm scale and (a′−d′) corresponding HR-TEM images on a 10 nm scale.

and (004) planes, respectively, correspond to the monoclinic phase of CuO and correlated with JCPDS card 48-1548.[39−41] Upon doping, the peaks were identical, attributed to a small amount of dopants being incorporated into the host material. The average crystallite sizes for CuO (13−15 nm) and CNC (10−11 nm) were calculated using the Scherrer equation. Furthermore, the interplanar spacing calculated with the Bragg equation was 0.35 nm for CNC and 0.27, 0.34, and 0.27 nm for undoped and CuO-doped samples. Figure 2b−e shows SAED patterns with ring characteristics formed by bright spots, corresponding to XRD data.

FTIR was employed to determine the presence of different functional groups in the 4000−450 cm^{-1} range (Figure 2f). The observed spectra for CuO and CNC exhibited transmittance peaks in the region 3000−3500 cm^{-1} corresponding to O−H stretching vibrations. Peaks recorded at around 1635 and 1435 cm^{-1} are correspondingly related to C═O and C−H_2 stretching vibrations that could be attributed to the

https://doi.org/10.1021/acsomega.2c00240
ACS Omega 2022, 7, 17043−17054

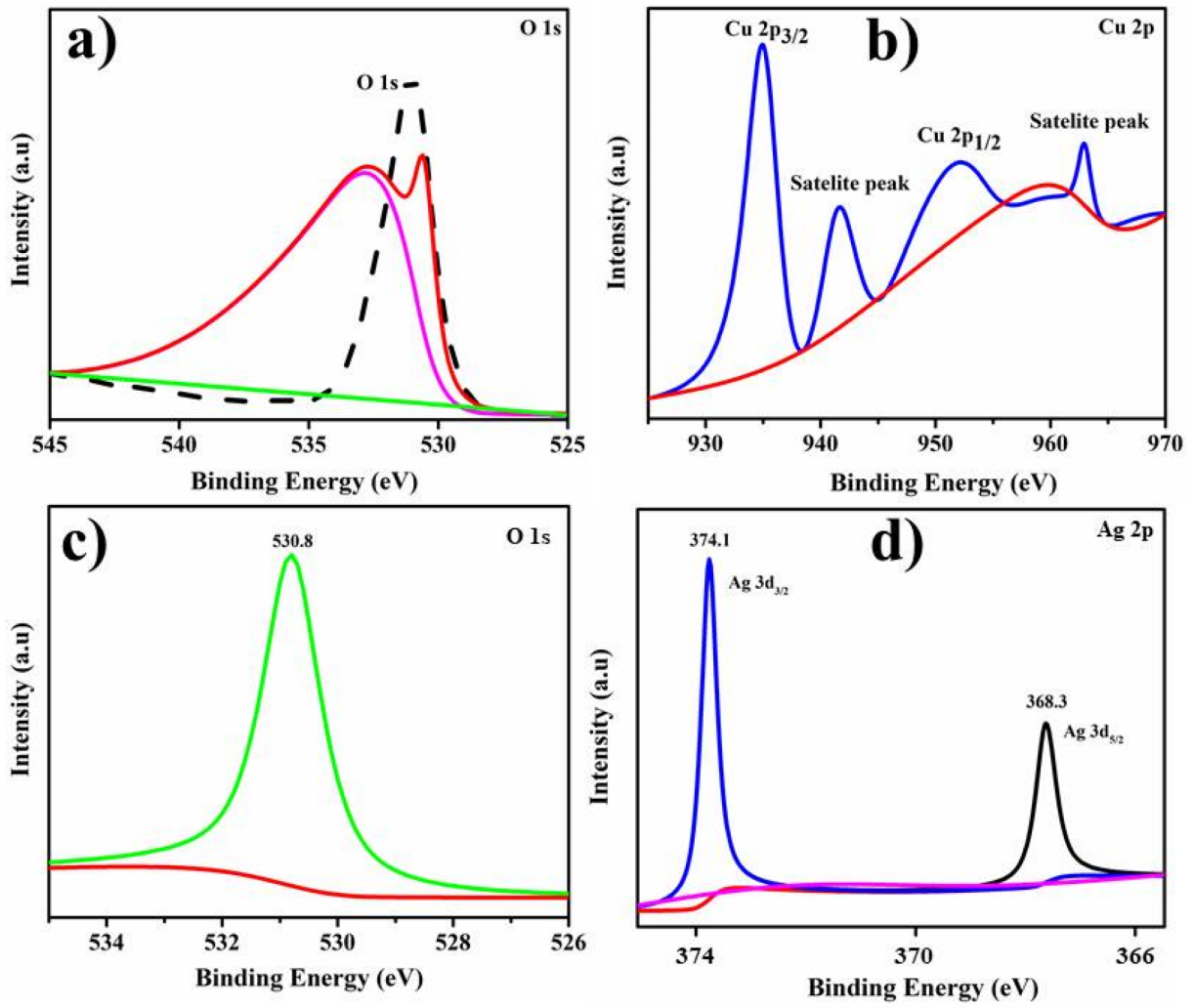

Figure 5. XPS spectra of binary doped CuO: (a) CuO O 1s; (b) Cu 2p; (c) Ag O 1s; (d) Ag 2p.

crystalline nature of CNC.[42−44] The observed peak in the range of 1019−1142 cm^{-1} illustrates the presence of sulfate ester bonds (C−O═S), which are induced by the hydrolysis of H_2SO_4 during CNC preparation.[44] For CuO and doped CuO, peaks at 1640 and 1502 cm^{-1} may indicate carbonyl C═O stretching, while the peak at 1371 cm^{-1} corresponds to C−O stretching of a carboxylate ion bonded to CuO as a bidentate ligand.[45,46] The band at around 1102 cm^{-1} was ascribed to a OH bending vibration due to excess hydroxyl groups.[17] The bands observed at 518 and 620 cm^{-1} are ascribed to the characteristic stretching vibrations of Cu−O bond formation, which confirmed the presence of a nanosized monoclinic phase of CuO.[45,46] Upon the addition of binary dopants, a minor shift in the transmittance peak toward a low wavenumber can be attributed to an alteration in Cu−O bond strength.[34]

To determine the optical properties of synthesized Ag-doped CNC-CuO nanomaterials, UV−vis spectroscopy was utilized (Figure 3a). The acquired spectra displayed characteristic absorption bands of 310−400 and 350−600 nm ranging from the UV to the visible region for CNC and CuO, respectively (Figure 3a). High-intensity peaks at 350 nm (CNC) and 360 nm (CuO) were recorded and attributed to the electronic transition from n to π^* molecular orbitals of CuO.[37,47] In addition, a slight bathochromic shift (toward longer wavelength) was observed in the absorption spectra upon doping, corresponding to a decrease in band-gap energy (E_g) and an increase in the crystallite size of CuO. The E_g values of pristine and doped CNC:CuO were obtained via a Tauc plot between $(\alpha h\nu)^2$ vs $h\nu$, as presented in Figure 3b. E_g values for CNC (3.15 eV) and CuO (2.5 eV) were measured, which matched well with the reported values.[37,48,49] Upon doping, a reduction in E_g to 2.45 eV for CNC-CuO and 2.4 eV for Ag/CNC-CuO was observed. The red shift is responsible for the decrease in band gap, most probably due to lattice distortions, electron−phonon coupling, and charge carrier localization.[14]

To analyze the exciton migration phenomenon and the presence of the inherent defects of reference and codoped CuO, PL was employed at room temperature with 280 nm excitation and 325−525 nm emission ranges (Figure 3c). CNC exhibited an intense PL emission band located in the 325−550 nm range under excitation at 300 nm, as delineated in Figure 3c.[50] The UV emission peak recorded at ∼360 nm is ascribed to e^-−h^+ recombination in free excitons, and visible emission peaks at 400 and 440 nm in the violet and blue regions, respectively, are ascribed to the near-band-edge emission (NBE) of the CuO nanostructure due to defects present in CuO.[51,52] A tiny luminescence peak at 486 nm is caused by the transition vacancy of interstitial oxygen.[51] The luminescence characteristics of CuO are strongly dependent upon the

https://doi.org/10.1021/acsomega.2c00240
ACS Omega 2022, 7, 17043−17054

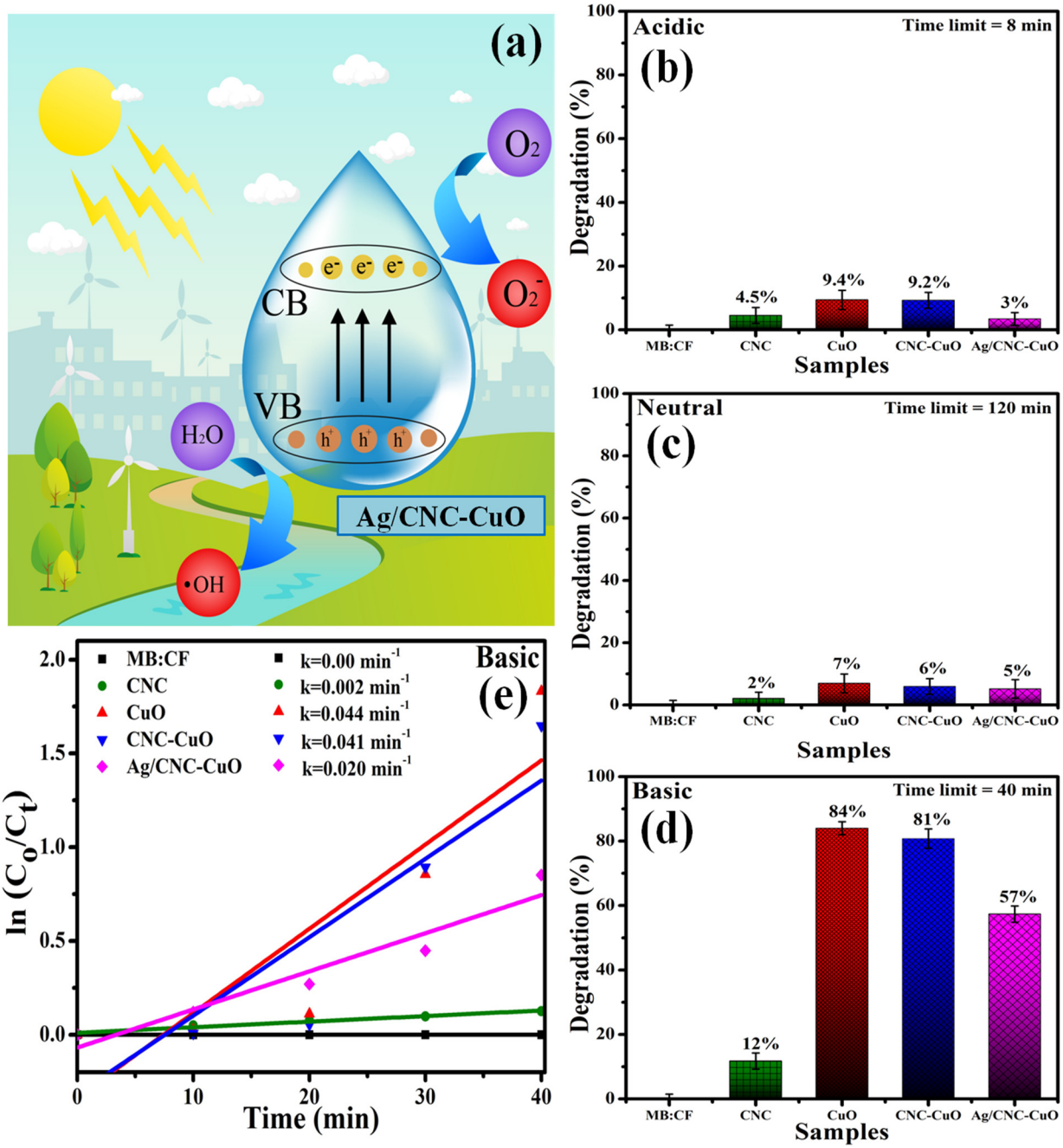

Figure 6. (a) Schematic illustration of photocatalytic activity. Photodegradation (%) in (b) acidic, (c) neutral, and (d) basic media. (e) Rate constants (basic) of Ag/CNC-CuO nanorods.

morphology of CuO, and surface contaminants may be formed during the transition of a mixed-phase crystal structure to a CuO crystalline structure.[51] An increase in luminescence intensity observed for binary-doped CuO is attributed to increasing intrinsic defect formation in the sample.[53]

The morphological features and crystal structures of doped and undoped CuO were characterized via HR-TEM, and the corresponding images at different scales are shown in Figure 4a−d,a′−d′). Figure 4a,a′ represents the formation of CNC NPs, and Figure 4b,b′ shows the formation of CuO nanorods (NRs), while Figure 4c,c′,d,d′ demonstrates an increase in length and diameter of the NRs with the incorporation of Ag/CNC. It seemed that Ag/CNC was connected with CuO, and agglomeration occurred in the doped materials, which eventually influenced the size of NRs. This increase in size offers an increased number of active sites for reactants, thus enhancing the antimicrobial activity. The corresponding SEM micrographs are also shown in Figure S3.

XPS was used to study the Ag and doped CuO surface elemental compositions, surface conditions, and binding energy shifts, see Figure 5. The high-resolution spectra of O 1s and Cu 2p are shown in Figure 5a,b. The O 1s spectrum revealed 529.18 and 531.08 eV binding energies, respectively, which relate to CuO (Figure 5a).[54] Primarily, Figure 5b specified the Cu 2p spectra of doped CuO containing peaks at binding energies of 933.3 and 953.3 eV ascribed to Cu $2p_{3/2}$ and Cu $2p_{1/2}$ spin orbitals, respectively, indicating the samples' divalent oxidation state. The other two peaks at 942.2 and 962

https://doi.org/10.1021/acsomega.2c00240
ACS Omega 2022, 7, 17043−17054

eV are ascribed to Cu $2p_{3/2}$ and Cu $2p_{1/2}$ satellite peaks, respectively, which appeared primarily in a divalent oxidation state of partly filled $3d_9$ orbitals.[55] The O 1s spectrum's greater peak at 530.8 eV is attributed to chemisorbed oxygen at the silver base.[56] The greater binding energy of O 1s in Ag is attributed to exposure to the air, although this binding energy is quite similar to that of a species identified as subsurface O in silver with a binding energy of 531.2 eV.[57] The XPS measurements specifically demonstrate the existence of metallic silver in the fresh sample, with binding energies of 368.3 and 374.1 eV for Ag $3d_{5/2}$ and Ag $3d_{3/2}$, respectively.[58]

To determine the catalytic activity of prepared samples in the presence of $NaBH_4$ (reducing agent) MB:CF was used as a targeted contaminant (Figures S1, S7, and S8). The degradation performance of samples was assessed between 200 and 900 nm via UV−vis spectroscopy at room temperature in different media (acidic, basic, neutral) by varying the pH. MB:CF exhibited an absorption peak at ∼665 nm in an aqueous solution. In the absence of nanocatalysts, MB:CF reduction with $NaBH_4$ showed only 0.1% degradation in 40 min, while the addition of nanocatalysts manifested a significant decrease in the concentration of MB:CF (Figure S1a−d. Bare and doped CNC and CuO nanocatalysts demonstrated efficient catalytic activity at pH ∼7 in the presence of $NaBH_4$ and degraded about 16% (8 min) 90% (1 min), 96% (2 min), and 97% (3 min) of the dye, respectively. Almost 100% degradation was observed in an acidic medium within 1, 1, and 3 min, respectively, for pristine and codoped CuO, while CNC manifested an 18% degradation efficiency (8 min). However, poor catalytic reduction was observed in a basic medium for all samples, showing only 7%, 7%, 5%, and 10% dye degradation.

The degradation mechanism of MB:CF to Leuco MB:CF involves NRs acting as electron relay to initiate electrons shifting from BH_4^- ions (donor) to dye molecules (acceptor). A large surface area of NRs enhances adsorption by offering abundant active sites for BH_4^- ions and dye molecules to simultaneously react with each other.[59,60] The degradation performance of nanocatalysts is also dependent on the pH of targeted dye.[61] Upon adding H_2SO_4 to create an acidic medium, more H^+ ions are available to be adsorbed on the surface of NRs to enhance catalytic activity. An increase in solution pH by adding NaOH increases the number of hydroxyl group,s resulting in oxidation of LMB:CF, hence decreasing the catalytic activity. Also, an electrostatic attraction between highly reactive OH^- ions and H atoms supplied by the reducing agent results in the formation of H_2O molecules, leaving the dye intact.[61,62] Consequently, the results demonstrated that the catalytic activity of nanocatalysts in acidic environments is significantly greater than that under alkaline conditions. Moreover, an increase in the catalytic activity of CuO was observed upon Ag-CNC doping in all mediums caused by an increase in active site number with doping. In conclusion, experimental results undoped and doped CuO NRs appear to show them to be suitable nanocatalysts for degrading dyes in industrial discharges. A literature comparison of the synthesized CuO NRs with other nanocatalysts under various conditions is also demonstrated in Table S1.

The photocatalytic potential of the metal oxide nanocomposite for reduction of MB:CF was evaluated under visible light irradiation in different media (acidic, neutral, basic) for 8, 120, and 40 min, respectively (Figures S9 and S10). In the absence of nanomaterials, the negligible reduction of MB:CF indicated that the dye gains stability with time and is hardly reduced. However, the addition of CNC, CuO, CNC-CuO, and Ag/CNC-CuO to an acidic medium displayed 4%, 9%, 9%, and 3% reduction in MB:CF concentration, respectively (Figure 6b). In neutral solution, only 2%, 7%, 6%, and 5% degradation efficiency was recorded for doped and undoped nanocatalysts, as demonstrated in Figure 6c. However, the dye degradation under alkaline conditions was 12%, 84%, 81%, and 57% for bare and codoped samples, respectively (Figure 6d)

In comparison, maximum dye degradation with nanocatalysts is achieved in a basic medium. The rate constant (pseudo-first-order kinetics) in basic medium for CNC, CuO, CNC-CuO, and Ag/CNC-CuO samples was 0.002, 0.044, 0.041, and 0.020 min^{-1}, respectively (Figure 6e).

The photocatalytic dye degradation mechanism occurs in several steps: (i) adsorption of dye molecules on nanorod surfaces, (ii) photogeneration of electron−hole pairs in the catalyst, (iii) redox reactions occurring at the surface to produce reactive radical species, (iv) reaction of dye molecules with radical species to produce degraded products, and (v) desorption of products from the catalyst surface. The generated hydroxyl radicals and superoxide anions reduce MB:CF into nontoxic substances.[63] The basic photocatalytic mechanism of the Ag/CNC-CuO nanocatalyst (Figure 6a), is shown in reactions 1−5.

$$\text{Ag/CNC−CuO} + h\nu \rightarrow \text{Ag−CNC−CuO}(h^+ + e^-) \quad (1)$$

$$e^- + O_2 \rightarrow {}^{\bullet}O_2^- \quad (2)$$

$$h^+ + OH^- \rightarrow {}^{\bullet}OH \quad (3)$$

$${}^{\bullet}OH + \text{organic dye} \rightarrow \text{degradation products} \quad (4)$$

$${}^{\bullet}O_2^- + \text{organic dye} \rightarrow \text{degradation products} \quad (5)$$

The photocatalytic activity of nanocatalyst is influenced by the catalyst amount, dye concentration, contact time, temperature, and pH of the dye solution.[64,65]

In an acidic medium, the surface of NRs will be positively charged due to the surplus number of H^+ atoms, while in an alkaline medium, abundant OH^- ions will induce a negative charge on the surface of the catalyst. MB:CF, being cationic, will offer more absorption on the negatively charged surface and hence more degradation will occur in a basic medium.[63]

As a result of our findings, we believe nanocatalysts in a basic medium are robust during reactions that rapidly remove organic dyes from water. According to the above analysis, the greater degradation efficiency of CuO is ascribed to the formation of intermediate energy levels, causing a decrease in electron−hole pair recombination. At the same time, a reduction in activity was observed upon Ag-CNC doping. On addition of codopants on the CuO surface, sunlight utilization decreases and faster e^-−h^+ pair recombination occurs.[66] Table S2 compares various dyes with varying catalyst amounts and times.

The *in vitro* microbiocidal properties of the control and doped samples were investigated against *S. aureus* and *E. coli* with a well diffusion assay (Table S3). The extracted data indicated that each sample had antimicrobial activity toward both bacteria. A synergistic response was revealed among the prepared samples and measured inhibition zones. Significant inhibition areas ($P < 0.05$) at minimum and maximum concentrations for *E. coli* (3.30 mm and 4.45 mm) and *S.*

https://doi.org/10.1021/acsomega.2c00240
ACS Omega 2022, 7, 17043−17054

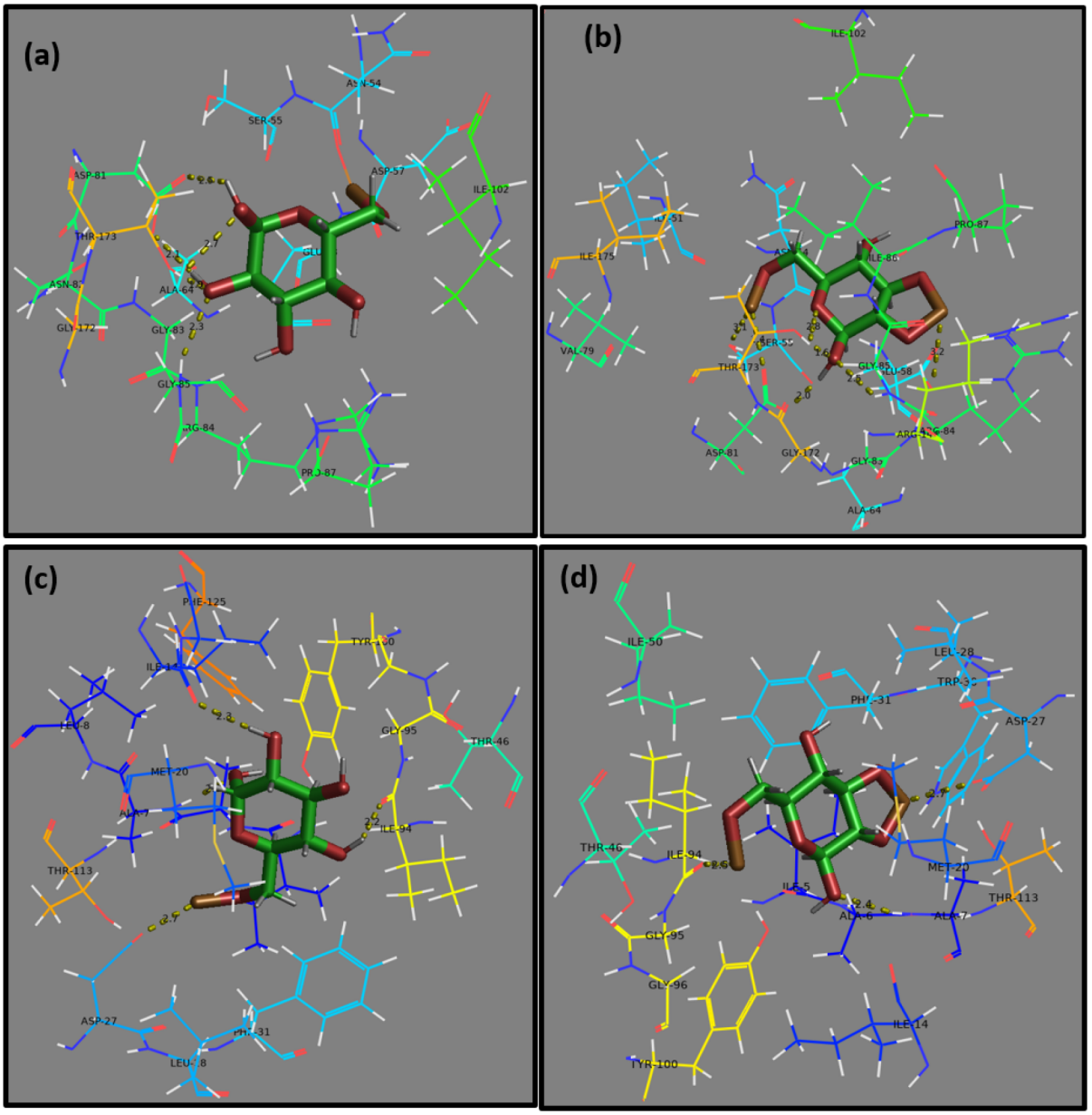

Figure 7. Binding interaction patterns of (a) CNC-CuO NRs, (b). Ag/CNC-CuO NRs with active site residues of DNA gyrase from *S. aureus*, (c) CNC-CuO NRs, and (d). Ag/CNC-CuO NRs with active site residues of DHFR from *E. coli*.

aureus (0.95 mm and 1.65 mm) were accomplished in the case of CNC in comparison with the positive control (7.10 and 9 mm, respectively). Moreover, for bare and codoped CuO, inhibition zones against *E. coli* in the ranges 1.35−2.40 and 2.25−3.45 mm and against *S. aureus* in the ranges 4.25−5.65 and 4.40−7.85 mm were recorded for both concentrations, respectively (Figure S11). Accordingly, all findings were compared to those obtained with ciprofloxacin (5.10 and 9 mm) and DI water (0 mm). Undoped and Co-doped CuO revealed superior microbicidal potential against G+ ve in comparison to G− bacteria while CNC manifested an intensified bactericidal response for G− compared with G+ bacteria. Co-doped CuO NRs efficiently supported bacteria-killing activity and exhibited significant antimicrobial potential, as depicted in Table S1.

Oxidative stress is determined by the form, size, and concentration of NRs in the prepared products. A reduction in the size of NRs correlates negatively with antibacterial effectiveness. Following the ejection of cytoplasmic contents, reactive oxygen species (ROS) created by nanosized rods encapsulate the microbial cell membrane, causing the bacteria to explode (see Figure S6).[67,68] Another reason for the response of binary doped CuO with bacteria strains is the important contact of cations with negatively charged regions of the bacterial membranes, resulting in the collapse of microorganisms. Cations included in the codoped material affect bacterial metabolic processes and degrade DNA cross-links. Additionally, cations impair bacterial ribosome action and cause enzymatic breakdown, culminating in the death of pathogens.[69]

In silico molecular docking studies have been reported as an attractive approach to unveil the mechanism behind the antibacterial activities of nanoparticles. Cellulose/TiO_2 NPs were previously reported to be potential antibacterial agents

https://doi.org/10.1021/acsomega.2c00240
ACS Omega 2022, 7, 17043−17054

having inhibitory activity against DHFR and DHPS enzymes of the folate biosynthetic pathway.[37] The exact mechanism behind the antibacterial activity of NPs still needs to be explored, and the use of *in silico* approaches for the prediction of possible targets is important. Here, dihydrofolate reductase (DHFR) and DNA gyrase, being well-known targets for antibiotics discovery, were selected as shown in Figure S2. Molecular docking predictions revealed the binding tendency and mechanism behind the inhibition potential of CNC-CuO and Ag/CNC-CuO NRs against selected enzymes.

In the case of DNA gyrase from *S. aureus*, the best-docked conformation for CNC-CuO NRs showed an H-bonding interaction with Asp81 (bond distances 2.1 and 2.5 Å), Thr173 (bond distances 1.9 and 2.7 Å), and Gly85 (bond distance 2.3 Å) with an overall binding score of −13.769 kcal/mol. Similarly, Ag/CNC-CuO NRs also showed good binding interaction patterns (binding score −14.591 kcal/mol) inside the active site of DNA gyrase enzyme for H-bonding with Glu58 (bond distance 3.2 Å), Thr173 (bond distances 1.6 and 2.8 Å), Ser55 (bond distance 3.1 Å), Arg85 (bond distance 2.5 Å), and Asp81 (bond distances 2.4 and 2.0 Å) (Figure 7a,b).

The best docking score for dihydrofolate reductase (DHFR) enzyme from *E. coli* was −9.718 kcal/mol, showing H-bonding interactions, i.e., Gly95 (bond distance 2.2 Å), Ile14 (bond distance 2.3 Å), Ala7 (bond distance 2.0 Å), and Asp27 (bond distance 2.7 Å) as the main contributors to the inhibition potential of CNC-CuO NRs. Similar interactions were observed for the binding of Ag/CNC-CuO NRs inside the active site of DHFR with a binding score of −7.993 kcal/mol having H-bonding interactions with Asp27 (bond distance 2.7 Å), Ala7 (bond distance 2.4 Å), and Ile94 (bond distance 2.5 Å), as depicted in Figure 7c,d.

In silico molecular docking studies predicted CNC-CuO NRs and Ag/CNC-CuO NRs to be potential inhibitors of DHFR and DNA gyrase enzyme and suggested inhibition of these enzymes as a possible mechanism behind the *in vitro* antibacterial activity.

4. CONCLUSION

Ag/CNC-CuO NRs were successfully synthesized in this study via a coprecipitation procedure with a target of increasing their antimicrobial, catalytic, and photocatalytic efficiency. An XRD analysis confirmed that no phase transformation in the monoclinic phase of CuO occurs upon codoping, and its interlayer *d* spacing (0.27 nm) is in agreement with the HR-TEM results. FTIR spectra showed Cu−O molecular bonding with diverse functional groups, with transmittance peaks of about 518 and 620 cm^{-1} in the fingerprint region. A red shift in the absorption band was observed in the range of 350−600 nm upon doping. An increase in PL intensity was attributed to fast electron−hole recombination and defect formation in the sample with codopants. Doping increased the formation of rods, which enhanced the antibacterial and catalytic activity, as shown by HR-TEM. An EDS analysis confirmed the effective doping of Ag-CNC into CuO with appropriate portions. On the basis of this study, the synthesized NRs showed outstanding antimicrobial efficacy against G+ and G− bacteria with codopants and unique catalytic (under acidic and neutral conditions) and photocatalytic (under basic conditions) response for use in contaminated water treatment and biomedical applications. Molecular docking studies predicted the inhibition of DHFR and DNA gyrase enzyme from *E. coli* and *S. aureus*, respectively, as a possible mechanism behind the *in vitro* bactericidal activity of CNC-CuO NRs and Ag/CNC-CuO NRs. NRs as possible antibiotics will be expanded if enzyme inhibition investigations prove their efficacy as antibacterial agents.

■ ASSOCIATED CONTENT

Supporting Information

The Supporting Information is available free of charge at https://pubs.acs.org/doi/10.1021/acsomega.2c00240.

Additional figures and tables, an experimental section, and an EDS analysis (PDF)

■ AUTHOR INFORMATION

Corresponding Authors

Muhammad Ikram − *Solar Cell Application Research Lab, Department of Physics, Government College University Lahore, Lahore 54000 Punjab, Pakistan;* orcid.org/0000-0001-7741-789X; Email: dr.muhammadikram@gcu.edu.pk

Anwar Ul-Hamid − *Core Research Facilities, King Fahd University of Petroleum & Minerals, Dhahran 31261, Saudi Arabia;* orcid.org/0000-0002-0259-301X; Email: anwar@kfupm.edu.sa

Walid Nabgan − *School of Chemical and Energy Engineering, Faculty of Engineering, Universiti Teknologi Malaysia, 81310 Skudai, Johor, Malaysia; Departament d'Enginyeria Química, Universitat Rovira i Virgili, 43007 Tarragona, Spain*; Email: wnabgan@gmail.com

Authors

Izan Hafeez − *Department of Physics, Riphah Institute of Computing and Applied Sciences (RICAS), Riphah International University, Lahore 54000, Pakistan*

Misbah Naz − *Department of Chemistry, Division of Science & Technology, University of Education, Lahore 54770, Pakistan*

Ali Haider − *Faculty of Veterinary and Animal Sciences, Muhammad Nawaz Shareef University of Agriculture, Multan 66000 Punjab, Pakistan*

Sadia Naz − *Tianjin Institute of Industrial Biotechnology, Chinese Academy of Sciences, Tianjin 300308, People's Republic of China*

Junaid Haider − *Tianjin Institute of Industrial Biotechnology, Chinese Academy of Sciences, Tianjin 300308, People's Republic of China*

Anum Shahzadi − *Faculty of Pharmacy, The University of Lahore, Lahore 54000, Pakistan*

Muhammad Imran − *State Key Laboratory of Chemical Resource Engineering, Beijing Advanced Innovation Centre for Soft Matter Science and Engineering, Beijing Engineering Center for Hierarchical Catalysts, Beijing University of Chemical Technology, Beijing 100029, People's Republic of China*

Salamat Ali − *Department of Physics, Riphah Institute of Computing and Applied Sciences (RICAS), Riphah International University, Lahore 54000, Pakistan*

Complete contact information is available at: https://pubs.acs.org/10.1021/acsomega.2c00240

Notes

The authors declare no competing financial interest.

https://doi.org/10.1021/acsomega.2c00240
ACS Omega 2022, 7, 17043−17054

■ ACKNOWLEDGMENTS

This work was supported by HEC Pakistan NRPU-project # 20-17615.

■ REFERENCES

(1) Wang, Z.; Wu, A.; Ciacchi, L. C.; Wei, G. Recent Advances in Nanoporous Membranes for Water Purification. *Nanomaterials* **2018**, *8* (2), 65.
(2) Dervin, S.; Dionysiou, D. D.; Pillai, S. C. 2D Nanostructures for Water Purification: Graphene and Beyond. *Nanoscale* **2016**, *8* (33), 15115−15131.
(3) Tlili, I.; Alkanhal, T. A. Nanotechnology for Water Purification: Electrospun Nanofibrous Membrane in Water and Wastewater Treatment. *J. Water Reuse Desalin.* **2019**, *9* (3), 232−247.
(4) Kimura, K.; Amy, G.; Drewes, J. E.; Heberer, T.; Kim, T. U.; Watanabe, Y. Rejection of Organic Micropollutants (Disinfection by-Products, Endocrine Disrupting Compounds, and Pharmaceutically Active Compounds) by NF/RO Membranes. *J. Membr. Sci.* **2003**, *227* (1−2), 113−121.
(5) Ikram, M.; Hussain, I.; Hassan, J.; Haider, A.; Imran, M.; Aqeel, M.; Ul-Hamid, A.; Ali, S. Evaluation of Antibacterial and Catalytic Potential of Copper-Doped Chemically Exfoliated Boron Nitride Nanosheets. *Ceram. Int.* **2020**, *46* (13), 21073−21083.
(6) Han, S.; Liu, K.; Hu, L.; Teng, F.; Yu, P.; Zhu, Y. Superior Adsorption and Regenerable Dye Adsorbent Based on Flower-Like Molybdenum Disulfide Nanostructure. *Sci. Rep.* **2017**, *7* (March), 1−11.
(7) Junaid, M.; Imran, M.; Ikram, M.; Naz, M.; Aqeel, M.; Afzal, H.; Majeed, H.; Ali, S. The Study of Fe-Doped CdS Nanoparticle-Assisted Photocatalytic Degradation of Organic Dye in Wastewater. *Appl. Nanosci.* **2019**, *9* (8), 1593−1602.
(8) Chowdhury, S.; Saha, P. Adsorption Kinetic Modeling of Safranin onto Rice Husk Biomatrix Using Pseudo-First- and Pseudo-Second-Order Kinetic Models: Comparison of Linear and Non-Linear Methods. *Clean - Soil, Air, Water* **2011**, *39* (3), 274−282.
(9) Rakshit, S.; Sarkar, D.; Elzinga, E. J.; Punamiya, P.; Datta, R. Mechanisms of Ciprofloxacin Removal by Nano-Sized Magnetite. *J. Hazard. Mater.* **2013**, *246−247*, 221−226.
(10) Shehu Imam, S.; Adnan, R.; Mohd Kaus, N. H. Photocatalytic Degradation of Ciprofloxacin in Aqueous Media: A Short Review. *Toxicol. Environ. Chem.* **2018**, *100* (5−7), 518−539.
(11) Geetha, M. P.; Pratheeksha, P.; Subrahmanya, B. K. Development of Functionalized CuO Nanoparticles for Enhancing the Adsorption of Methylene Blue Dye. *Cogent Eng.* **2020**, *7* (1), 1783102.
(12) Ranson, M.; Cox, B.; Keenan, C.; Teitelbaum, D. The Impact of Pollution Prevention on Toxic Environmental Releases from U.S. Manufacturing Facilities. *Environ. Sci. Technol.* **2015**, *49* (21), 12951−12957.
(13) Bethi, B.; Sonawane, S. H.; Bhanvase, B. A.; Gumfekar, S. P. Nanomaterials-Based Advanced Oxidation Processes for Wastewater Treatment: A Review. *Chem. Eng. Process. Process Intensif.* **2016**, *109*, 178−189.
(14) Iqbal, S.; Javed, M.; Bahadur, A.; Qamar, M. A.; Ahmad, M.; Shoaib, M.; Raheel, M.; Ahmad, N.; Akbar, M. B.; Li, H. Controlled Synthesis of Ag-Doped CuO Nanoparticles as a Core with Poly(Acrylic Acid) Microgel Shell for Efficient Removal of Methylene Blue under Visible Light. *J. Mater. Sci. Mater. Electron.* **2020**, *31* (11), 8423−8435.
(15) Rajeshwar, K. Solar Energy Conversion and Environmental Remediation Using Inorganic Semiconductor-Liquid Interfaces: The Road Traveled and the Way Forward. *J. Phys. Chem. Lett.* **2011**, *2* (11), 1301−1309.
(16) Zhang, X.; Suo, H.; Zhang, R.; Niu, S.; Qi Zhao, X.; Zheng, J.; Guo, C. Photocatalytic Activity of 3D Flower-like MoS2 Hemispheres. *Mater. Res. Bull.* **2018**, *100* (2010), 249−253.
(17) Muthuvel, A.; Jothibas, M.; Manoharan, C. Synthesis of Copper Oxide Nanoparticles by Chemical and Biogenic Methods: Photocatalytic Degradation and in Vitro Antioxidant Activity. *Nanotechnol. Environ. Eng.* **2020**, *5* (2), 1−19.
(18) Pal, D. B.; Giri, D. D.; Singh, P.; Bhargav, M. Synthesis and Characterization of CuO Nanoparticles by Aqueous Precipitation Method. *2nd Int. Conf. Nanotechnol.* 2015, *3* (8).
(19) Jillani, S.; Jelani, M.; Hassan, N. U.; Ahmad, S.; Hafeez, M. Synthesis, Characterization and Biological Studies of Copper Oxide Nanostructures. *Mater. Res. Express* **2018**, *5* (4), 045006.
(20) Habiba, U.; Islam, M. S.; Siddique, T. A.; Afifi, A. M.; Ang, B. C. Adsorption and Photocatalytic Degradation of Anionic Dyes on Chitosan/PVA/Na-Titanate/TiO2 Composites Synthesized by Solution Casting Method. *Carbohydr. Polym.* **2016**, *149*, 317−331.
(21) Valencia, L.; Kumar, S.; Nomena, E. M.; Salazar-Alvarez, G.; Mathew, A. P. In-Situ Growth of Metal Oxide Nanoparticles on Cellulose Nanofibrils for Dye Removal and Antimicrobial Applications. *ACS Appl. Nano Mater.* **2020**, *3* (7), 7172−7181.
(22) Lizundia, E.; Puglia, D.; Nguyen, T. D.; Armentano, I. Cellulose Nanocrystal Based Multifunctional Nanohybrids. *Prog. Mater. Sci.* **2020**, *112*, 100668.
(23) Fu, F.; Gu, J.; Cao, J.; Shen, R.; Liu, H.; Zhang, Y.; Liu, X.; Zhou, J. Reduction of Silver Ions Using an Alkaline Cellulose Dope: Straightforward Access to Ag/ZnO Decorated Cellulose Nanocomposite Film with Enhanced Antibacterial Activities. *ACS Sustain. Chem. Eng.* **2018**, *6* (1), 738−748.
(24) Tsai, T. T.; Huang, T. H.; Chang, C. J.; Yi-Ju Ho, N.; Tseng, Y. T.; Chen, C. F. Antibacterial Cellulose Paper Made with Silver-Coated Gold Nanoparticles. *Sci. Rep.* **2017**, *7* (1), 1−10.
(25) Wang, S.; Lu, A.; Zhang, L. Recent Advances in Regenerated Cellulose Materials. *Prog. Polym. Sci.* **2016**, *53*, 169−206.
(26) Zhang, F.; Ren, H.; Dou, J.; Tong, G.; Deng, Y. Cellulose Nanofibril Based-Aerogel Microreactors: A High Efficiency and Easy Recoverable W/O/W Membrane Separation System. *Sci. Rep.* **2017**, *7*, 1−7.
(27) Kaushik, M.; Moores, A. Review: Nanocelluloses as Versatile Supports for Metal Nanoparticles and Their Applications in Catalysis. *Green Chem.* **2016**, *18* (3), 622−637.
(28) Elfeky, A. S.; Salem, S. S.; Elzaref, A. S.; Owda, M. E.; Eladawy, H. A.; Saeed, A. M.; Awad, M. A.; Abou-Zeid, R. E.; Fouda, A. Multifunctional Cellulose Nanocrystal /Metal Oxide Hybrid, Photo-Degradation, Antibacterial and Larvicidal Activities. *Carbohydr. Polym.* **2020**, *230*, 115711.
(29) Nath, B. K.; Chaliha, C.; Kalita, E.; Kalita, M. C. Synthesis and Characterization of ZnO:CeO2:Nanocellulose:PANI Bionanocomposite. A Bimodal Agent for Arsenic Adsorption and Antibacterial Action. *Carbohydr. Polym.* **2016**, *148*, 397−405.
(30) Du, M.; Du, Y.; Feng, Y.; Yang, K.; Lv, X.; Jiang, N.; Liu, Y. Facile Preparation of BiOBr/Cellulose Composites by in Situ Synthesis and Its Enhanced Photocatalytic Activity under Visible-Light. *Carbohydr. Polym.* **2018**, *195* (April), 393−400.
(31) Mavaei, M.; Chahardoli, A.; Shokoohinia, Y.; Khoshroo, A.; Fattahi, A. One-Step Synthesized Silver Nanoparticles Using Isoimperatorin: Evaluation of Photocatalytic, and Electrochemical Activities. *Sci. Rep.* **2020**, *10* (1), 1−12.
(32) Babu, A. T.; Antony, R. Green Synthesis of Silver Doped Nano Metal Oxides of Zinc & Copper for Antibacterial Properties, Adsorption, Catalytic Hydrogenation & Photodegradation of Aromatics. *J. Environ. Chem. Eng.* **2019**, *7* (1), 102840.
(33) Absike, H.; Hajji, M.; Labrim, H.; Abbassi, A.; Ez-Zahraouy, H. Electronic, Electrical and Optical Properties of Ag Doped CuO through Modified Becke-Johnson Exchange Potential. *Superlattices Microstruct.* **2019**, *127*, 128−138.
(34) Thakur, N.; Anu Kumar, K. Effect of (Ag, Co) Co-Doping on the Structural and Antibacterial Efficiency of CuO Nanoparticles: A Rapid Microwave Assisted Method. *J. Environ. Chem. Eng.* **2020**, *8* (4), 104011.
(35) Lizundia, E.; Goikuria, U.; Vilas, J. L.; Cristofaro, F.; Bruni, G.; Fortunati, E.; Armentano, I.; Visai, L.; Torre, L. Metal Nanoparticles Embedded in Cellulose Nanocrystal Based Films: Material Properties and Post-Use Analysis. *Biomacromolecules* **2018**, *19* (7), 2618−2628.

https://doi.org/10.1021/acsomega.2c00240
ACS Omega 2022, 7, 17043−17054

(36) Phiwdang, K.; Suphankij, S.; Mekprasart, W.; Pecharapa, W. Synthesis of CuO Nanoparticles by Precipitation Method Using Different Precursors. *Energy Procedia* **2013**, *34*, 740−745.
(37) Arularasu, M. V.; Harb, M.; Sundaram, R. Synthesis and Characterization of Cellulose/TiO2 Nanocomposite: Evaluation of in Vitro Antibacterial and in Silico Molecular Docking Studies. *Carbohydr. Polym.* **2020**, *249*, 116868.
(38) Saska, S.; Barud, H. S.; Gaspar, A. M. M.; Marchetto, R.; Ribeiro, S. J. L.; Messaddeq, Y. Bacterial Cellulose-Hydroxyapatite Nanocomposites for Bone Regeneration. *Int. J. Biomater.* **2011**, *2011*, 1.
(39) Ethiraj, A. S.; Kang, D. J. Synthesis and Characterization of CuO Nanowires by a Simple Wet Chemical Method. *Nanoscale Res. Lett.* **2012**, *7*, 1−5.
(40) Tan, J.; Dun, M.; Li, L.; Zhao, J.; Li, X.; Hu, Y.; Huang, G.; Tan, W.; Huang, X. Self-Template Derived CuO Nanowires Assembled Microspheres and Its Gas Sensing Properties. *Sensors Actuators, B Chem.* **2017**, *252*, 1−8.
(41) Wang, L.; Zhang, K.; Hu, Z.; Duan, W.; Cheng, F.; Chen, J. Porous CuO Nanowires as the Anode of Rechargeable Na-Ion Batteries. *Nano Res.* **2014**, *7* (2), 199−208.
(42) Tang, C.; Wang, Y.; Long, Y.; An, X.; Shen, J.; Ni, Y. Anchoring 20(R)-Ginsenoside Rg3 onto Cellulose Nanocrystals to Increase the Hydroxyl Radical Scavenging Activity. *ACS Sustain. Chem. Eng.* **2017**, *5* (9), 7507−7513.
(43) Taheri, A.; Mohammadi, M. The Use of Cellulose Nanocrystals for Potential Application in Topical Delivery of Hydroquinone. *Chem. Biol. Drug Des.* **2015**, *86* (1), 102−106.
(44) Jayaramudu, T.; Ko, H. U.; Kim, H. C.; Kim, J. W.; Muthoka, R. M.; Kim, J. Electroactive Hydrogels Made with Polyvinyl Alcohol/Cellulose Nanocrystals. *Materials (Basel).* **2018**, *11* (9), 1615.
(45) Jeronsia, J. E.; Vidhya Raj, D. J.; Joseph, L. A.; Rubini, K.; Das, S. J. In Vitro Antibacterial and Anticancer Activity of Copper Oxide Nanostructures in Human Breast Cancer Michigan Cancer Foundation-7 Cells. *J. Med. Sci.* **2016**, *36* (4), 145−151.
(46) Dhineshbabu, N. R.; Rajendran, V.; Nithyavathy, N.; Vetumperumal, R. Study of Structural and Optical Properties of Cupric Oxide Nanoparticles. *Appl. Nanosci.* **2016**, *6* (6), 933−939.
(47) Tadjarodi, A.; Akhavan, O.; Bijanzad, K. Photocatalytic Activity of CuO Nanoparticles Incorporated in Mesoporous Structure Prepared from Bis(2-Aminonicotinato) Copper(II) Microflakes. *Trans. Nonferrous Met. Soc. China (English Ed.* **2015**, *25* (11), 3634−3642.
(48) Mousali, E.; Zanjanchi, M. A. Electrochemical Synthesis of Copper(II) Oxide Nanorods and Their Application in Photocatalytic Reactions. *J. Solid State Electrochem.* **2019**, *23* (3), 925−935.
(49) Yang, C.; Su, X.; Xiao, F.; Jian, J.; Wang, J. Gas Sensing Properties of CuO Nanorods Synthesized by a Microwave-Assisted Hydrothermal Method. *Sensors Actuators, B Chem.* **2011**, *158* (1), 299−303.
(50) Nedilko, S. G.; Revo, S. L.; Chornii, V. P.; Scherbatskyi, V. P.; Nedielko, M. S. Luminescent Determination of Nitrite Traces in Water Solutions Using Cellulose as Sorbent. *J. Sensors Sens. Syst.* **2015**, *4* (1), 31−36.
(51) Wang, Y.; Jiang, T.; Meng, D.; Kong, J.; Jia, H.; Yu, M. Controllable Fabrication of Nanostructured Copper Compound on a Cu Substrate by a One-Step Route. *RSC Adv.* **2015**, *5* (21), 16277−16283.
(52) Iqbal, M.; Ali, A.; Ahmad, K. S.; Rana, F. M.; Khan, J.; Khan, K.; Thebo, K. H. Synthesis and Characterization of Transition Metals Doped CuO Nanostructure and Their Application in Hybrid Bulk Heterojunction Solar Cells. *SN Appl. Sci.* **2019**, *1* (6), 1−8.
(53) Singh, B. P.; Chaudhary, M.; Kumar, A.; Singh, A. K.; Gautam, Y. K.; Rani, S.; Walia, R. Effect of Co and Mn Doping on the Morphological, Optical and Magnetic Properties of CuO Nanostructures. *Solid State Sci.* **2020**, *106*, 106296.
(54) Baig, N.; Saleh, T. A. Superhydrophobic Polypropylene Functionalized with Nanoparticles for Efficient Fast Static and Dynamic Separation of Spilled Oil from Water. *Glob. Challenges* **2019**, *3* (8), 1800115.
(55) Poulston, S.; Parlett, P. M.; Stone, P.; Bowker, M. Surface Oxidation and Reduction of CuO and Cu2O Studied Using XPS and XAES. *Surf. Interface Anal.* **1996**, *24* (12), 811−820.
(56) El Mel, A. A.; Stephant, N.; Hamon, J.; Thiry, D.; Chauvin, A.; Chettab, M.; Gautron, E.; Konstantinidis, S.; Granier, A.; Tessier, P. Y. Creating Nanoporosity in Silver Nanocolumns by Direct Exposure to Radio-Frequency Air Plasma. *Nanoscale* **2016**, *8* (1), 141−148.
(57) Boronin, A. I.; Bukhityarov, V. I.; Vishnevskii, A. L.; Boreskov, G. K.; Savchenko, V. I. XPS and UPS Studies of Oxygen Adsorption over Clean and Carbon-Modified Silver Surfaces. *Surf. Sci.* **1988**, *201* (1−2), 195−210.
(58) Ghosh, S.; Acharyya, S. S.; Sasaki, T.; Bal, R. Room Temperature Selective Oxidation of Aniline to Azoxybenzene over a Silver Supported Tungsten Oxide Nanostructured Catalyst. *Green Chem.* **2015**, *17* (3), 1867−1876.
(59) Ikram, M.; Tabassum, R.; Qumar, U.; Ali, S.; Ul-Hamid, A.; Haider, A.; Raza, A.; Imran, M.; Ali, S. Promising Performance of Chemically Exfoliated Zr-Doped MoS2nanosheets for Catalytic and Antibacterial Applications. *RSC Adv.* **2020**, *10* (35), 20559−20571.
(60) Fairuzi, A. A.; Bonnia, N. N.; Akhir, R. M.; Abrani, M. A.; Akil, H. M. Degradation of Methylene Blue Using Silver Nanoparticles Synthesized from Imperata Cylindrica Aqueous Extract. *IOP Conf. Ser. Earth Environ. Sci.* **2018**, *105* (1), 012018.
(61) Boumediene, M.; Benaïssa, H.; George, B.; Molina, S.; Merlin, A. Effects of PH and Ionic Strength on Methylene Blue Removal from Synthetic Aqueous Solutions by Sorption onto Orange Peel and Desorption Study. *J. Mater. Environ. Sci.* **2018**, *9* (6), 1700−1711.
(62) Zhou, S.; Du, Z.; Li, X.; Zhang, Y.; He, Y.; Zhang, Y. Degradation of Methylene Blue by Natural Manganese Oxides: Kinetics and Transformation Products. *R. Soc. Open Sci.* **2019**, *6* (7), 190351.
(63) Kaur, H.; Kumar, S.; Verma, N. K.; Singh, P. Role of PH on the Photocatalytic Activity of TiO2 Tailored by W/T Mole Ratio. *J. Mater. Sci. Mater. Electron.* **2018**, *29* (18), 16120−16135.
(64) Guillard, C.; Lachheb, H.; Houas, A.; Ksibi, M.; Elaloui, E.; Herrmann, J. M. Influence of Chemical Structure of Dyes, of PH and of Inorganic Salts on Their Photocatalytic Degradation by TiO2 Comparison of the Efficiency of Powder and Supported TiO2. *J. Photochem. Photobiol. A Chem.* **2003**, *158* (1), 27−36.
(65) Kumar, A. A Review on the Factors Affecting the Photocatalytic Degradation of Hazardous Materials. *Mater. Sci. Eng. Int. J.* **2017**, *1* (3), 106.
(66) Kadam, A. N.; Kim, T. G.; Shin, D. S.; Garadkar, K. M.; Park, J. Morphological Evolution of Cu Doped ZnO for Enhancement of Photocatalytic Activity. *J. Alloys Compd.* **2017**, *710*, 102−113.
(67) Nagarajan, S.; Arumugam Kuppusamy, K. Extracellular Synthesis of Zinc Oxide Nanoparticle Using Seaweeds of Gulf of Mannar, India. *J. Nanobiotechnology* **2013**, *11* (1), 39.
(68) Haider, A.; Ijaz, M.; Imran, M.; Naz, M.; Majeed, H.; Khan, J. A.; Ali, M. M.; Ikram, M. Enhanced Bactericidal Action and Dye Degradation of Spicy Roots' Extract-Incorporated Fine-Tuned Metal Oxide Nanoparticles. *Appl. Nanosci.* **2020**, *10* (4), 1095−1104.
(69) Hosseinkhani, P.; Zand, A. M.; Imani, S.; Rezayi, M.; Rezaei Zarchi, S. Determining the Antibacterial Effect of ZnO Nanoparticle against the Pathogenic Bacterium, Shigella Dysenteriae (Type 1). *Int. J. Nano Dimens.* **2011**, *1* (4), 279−285.

https://doi.org/10.1021/acsomega.2c00240
ACS Omega 2022, 7, 17043−17054